

Vessels-Cut: A Graph Based Approach to Patient-Specific Carotid Arteries Modeling

Moti Freiman¹, Noah Broide¹, Miriam Natanzon¹, Einav Nammer²,
Ofek Shilon², Lior Weizman¹, Leo Joskowicz¹, and Jacob Sosna³

¹ School of Eng. and Computer Science, The Hebrew Univ. of Jerusalem, Israel

² Symbionix Ltd, Israel

³ Dept. Of Radiology, Hadassah Hebrew University Medical Center, Israel

freiman@cs.huji.ac.il

Abstract. We present a nearly automatic graph-based segmentation method for patient specific modeling of the aortic arch and carotid arteries from CTA scans for interventional radiology simulation. The method starts with morphological-based segmentation of the aorta and the construction of a prior intensity probability distribution function for arteries. The carotid arteries are then segmented with a graph min-cut method based on a new edge weights function that adaptively couples the voxel intensity, the intensity prior, and geometric vesselness shape prior. Finally, the same graph-cut optimization framework is used for nearly automatic removal of a few vessel segments and to fill minor vessel discontinuities due to highly significant imaging artifacts. Our method accurately segments the aortic arch, the left and right subclavian arteries, and the common, internal, and external carotids and their secondary vessels. It does not require any user initialization, parameters adjustments, and is relatively fast (150–470 secs). Comparative experimental results on 30 carotid arteries from 15 CTAs from two medical centres manually segmented by expert radiologist yield a mean symmetric surface distance of 0.79mm (std=0.25mm). The nearly automatic refinement requires about 10 seed points and took less than 2mins of treating physician interaction with no technical support for each case.

1 Introduction

Minimally invasive endovascular surgeries such as carotid, coronary, and cerebral angiographic procedures are frequent in interventional radiology. They require experienced physicians and involve time-consuming trial and error with repeated contrast agent injection and X-ray imaging. This leads to outcome variability and non-negligible complication rates. Training simulators such the ANGIO MentorTM (Symbionix Ltd, Israel) have the potential to significantly reduce the physicians' learning curve, reduce the outcome variability, and improve their performance. A key limitation is the simulators' reliance on hand-tailored anatomical models generated by a technician from CTA scans, which are impractical to produce patient-specific simulations in a clinical environment.

Carotid arteries segmentation from CTAs is a challenging task because of significant intra and inter-patient carotid intensity and geometry variance, intensity values overlap of carotid arteries and neck vertebrae, and streaking artifacts, among others. Numerous automatic and semi-automatic vascular structure segmentation methods have been developed recently [1]. The main approaches rely on intensity values [2], geometric shape [3], edge-based active contours [4,5], statistical active shape models [6], and contour tracking [7,8,9]. Since these segmentation algorithms have been developed for specific regions, such as the carotid bifurcation, their performance on the segmentation of the entire vascular anatomy often yield inaccurate vessel diameters, miss vessels segments and entire small vessels, include non-vessel anatomical structures, and incorrectly model vessel bifurcations and pathologies. These failures are often due to severe stenosis around the carotid bifurcation [8] and the local vessels appearance and characteristics variability in various regions of the body. In addition, most methods require extensive user interaction and expert technical support for the adjustment of non-intuitive parameters, which difficult their routine clinical use.

A promising approach is the graph min-cut segmentation method [10,11]. It classifies the voxel nodes that separate the objects of interest and the background based on weighted voxel adjacencies. The advantages of graph min-cut segmentation are that it is generic and that it is nearly parameter-free. However, it relies on significant user interaction and requires a technical expert to fine-tune the vessels intensity priors to capture the small vessels variability. It does not incorporate vessels geometric information, is computationally intensive, and has extensive memory requirements.

Recent improvements to the graph min-cut interactive segmentation method address some of these drawbacks. Slabaugh and Unal [12] add an elliptical shape prior term to the edges cost function. Sinop and Grady [13] use a Laplacian pyramid to accelerate the segmentation and to reduce the memory requirements. Ning et al. [14] improve the segmentation with graph-cut active contours based on prior object surface estimation. Rother et al [15] require user-defined enclosing rectangular regions around the objects of interest. While this method is useful for extracting simple objects in 2D images of natural scenes, it is laborious for 3D scans of complex vascular structures. A common key drawback of all these methods is that their generic segmentation framework is often ill-suited for volumetric vessels segmentation.

In this work we present a nearly automatic graph min-cut segmentation method for the carotid arteries and the aorta. It consists of automatic segmentation step followed by nearly automatic removal of few vein segments and filling minor vessel discontinuities due to large intensity variations. The main contributions of this work are: 1) a new graph-cut with tubular shape prior formulation for vessels segmentation, 2) a novel edge weights function that adaptively couples intensity with geometric vesselness shape prior, and; 3) a new nearly automatic method for segmentation of the entire carotids system.

The automatic step does not require any user initialization or parameters adjustment. It can segment the entire head and neck CTA scans ($512 \times 512 \times 750$

voxels) in 150–470secs, depending on the scan resolution. We then use the same graph-cut optimization framework to interactively remove a few vein segments and to fill minor vessel discontinuities due to large intensity variations. Experimental results on 30 carotid arteries from 15 scans from two medical centers show that our method is accurate, reliable, and fast enough to generate patient specific models for interventional radiology simulation with only 2mins of treating physician intervention and no technical support.

2 Method

Our segmentation method consists of: 1) automatic aortic arch segmentation, 2) automatic carotid, vertebral, and subclavian arteries segmentation, and; 3) interactive graph-based refinement. We describe each stage in detail next.

2.1 Aortic Arch Segmentation

The aorta is the dominant arch-like vessel above the pulmonary artery in the lower region of a head and neck CTA scan. Aortic arch segmentation relies on prior anatomical knowledge of the aortic arch structure: the aorta location, its estimated radius, and its relative brightness.

Our aortic arch segmentation algorithm starts with automatic Region of Interest (ROI) selection and enhancement, followed by morphological segmentation. The lower fourth of the CTA scan is first selected, downsampled (1:9), and smoothed with a Gaussian kernel (Fig. 1a). Next, background voxels whose values are outside the vessels intensity range (typically 0-600 HU) are eliminated. Finally, a log-based intensity transform is applied to enhance the dominant blood vessels and conceal small vessels (Fig. 1b). A morphological ellipsoid operator is then applied to the enhanced ROI. Each voxel is classified based on the high homogeneity and low number of background voxels of the ellipsoid voxel neighborhood whose dimensions are derived from the typical aorta radius.

The resulting classification includes three connected components: the aortic arch, the pulmonary artery, and the spinal cord. We grade these components by low variance and arch-like structure and choose the one with the highest score (Fig. 1c). Finally, mean and standard deviation aorta intensity values are computed for their use as prior Intensity Probability Distribution Function (IPDF).

2.2 Carotid Arteries Segmentation

We use a min-cut graph segmentation approach [10] to segment the arteries. We combine the estimated aorta IPDF, the geometric tube-like shape prior based on multi-scale Hessian eigen-analysis [3], and the local image gradients into a graph-based image volume representation.

Let $G = (V, E)$ be the image graph, where $V = \{v_1, \dots, v_n, v_s, v_t\}$ are the graph nodes such that node v_i corresponds to voxel i and terminal nodes v_s and v_t correspond to object and background, respectively. Graph edges

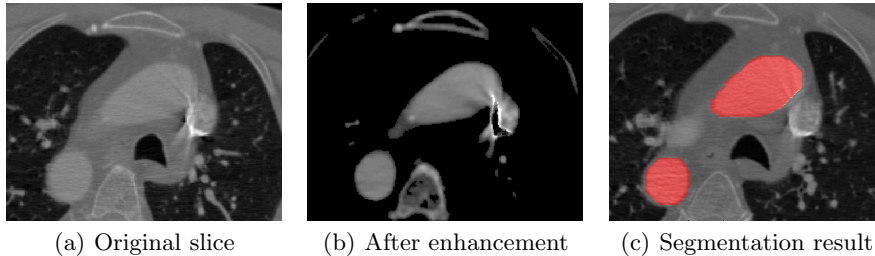


Fig. 1. Automatic aorta segmentation: (a) CTA scan axial slice after downsampling and smoothing; (b) enhanced image; (c) aortic arch segmentation

$E = \{(v_i, v_s), (v_i, v_t), (v_i, v_j)\}$ consist of: 1) edges (v_i, v_s) from voxels to the object terminal node; 2) edges (v_i, v_t) from voxels to the background terminal node, and; 3) edges (v_i, v_j) between adjacent voxels (4 or 8 neighbors for 2D images, 6 or 26 neighbors for 3D images). The cost of a cut $|C|$ that divides the graph into two parts, one associate with the source vertex (e.g. object class), and one associate with target vertex (e.g. background class) is defined as the sum of the weights of the cut edges $e \in C$. The segmentation is obtained by minimization of the cut cost:

$$\operatorname{argmin}_{e \in C} \sum_{e \in C} w_e \quad (1)$$

Edges weights (w_e) are assigned as follows. Edge weights $w(v_i, v_s)$ represent the posterior probability that voxel v_i is related to the vessels (object) or to the background (target):

$$w(v_i, v_s) = Pr(v_i \in I(O)) \cdot Pr(v_i \in S(O)) \quad (2)$$

where $Pr(v_i \in I(O))$ is the probability that the voxel belongs to the object class based on voxel's intensity v_i and object's IPDF $I(O)$. The term $Pr(v_i \in S(O))$ is the geometrical shape information prior of the current voxel computed using Frangi's multi-scale Hessian based vesselness filter [3]:

$$M(\sigma) = \begin{cases} 0 & \lambda_2 > 0 \text{ or} \\ & \lambda_3 > 0, \\ \left(1 - \exp\left(-\frac{R_A^2}{(2a)^2}\right)\right) \left(\exp\left(-\frac{R_B^2}{(2b)^2}\right)\right) \left(1 - \exp\left(-\frac{S^2}{(2c)^2}\right)\right) & \text{otherwise} \end{cases} \quad (3)$$

where

$$R_A = \frac{|\lambda_2|}{|\lambda_3|} \quad R_B = \frac{|\lambda_1|}{\sqrt{|\lambda_2 \lambda_3|}} \quad S = \sqrt{\lambda_1^2 + \lambda_2^2 + \lambda_3^2}$$

and σ is the scale at which the measure is computed. R_A differentiates between plate and line-like structures, R_B measures the deviation from blob-like structures, and S differentiates between foreground (vessel) and background (noise).

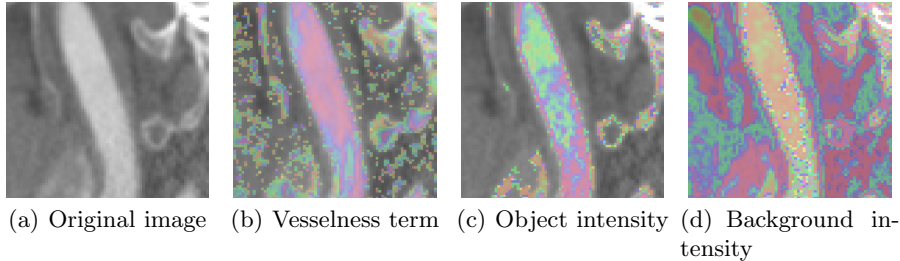


Fig. 2. Illustration of the new graph edge weights function: (a) original CTA sagittal slice; (b) shape-based probability map of each voxel to belong to the object class; (c-d) intensity based probability of each voxel to belong to the object (background) class. Red pixels denote high membership values.

Constants a , b and c are predefined weights determining the influence of R_A , R_B and S . The vesselness measure value is close to 1 for voxels with tube-like structures, and close to 0 otherwise. The vesselness measure is computed for each voxel and for each scale. Finally, for each voxel, the maximal value among the different scales is set to the vesselness measure for the voxel.

Edge weights $w(v_i, v_t)$ represent the probability of each voxel to belong to background class:

$$w(v_i, v_t) = Pr(v_i \in I(B)) \cdot Pr(v_i \notin S(O)) \quad (4)$$

where $Pr(v_i \in I(O))$ is the probability that the voxel belongs to the background class based on voxel's intensity v_i and background IPDF, implicitly computed as described by Freiman et al [16], and $Pr(v_i \notin S(O)) = 1 - Pr(v_i \in S(O))$.

Edges weight $w(v_i, v_j)$ represent the magnitude of the local gradient between the adjacent voxels:

$$w(v_i, v_j) = \exp\left(-\frac{(I(v_i) - I(v_j))^2}{\sigma(Pr(v_i \in S(O)))}\right) \quad (5)$$

where σ is linearly depend on the geometrical shape information $Pr(v_i \in S(O))$. The adaptive weighting is designed to cope with small intensity differences inside the vessels while accounting for these differences along the vessel surface. Fig. 2 illustrates the different weights of each voxel on a sagittal slice.

The coupling of both intensity and geometrical shape information yield a robust and accurate segmentation method that correctly segments both healthy and pathological cases with mild or severe stenosis and calcifications without any parameter tuning. Fig. 3 illustrates the performance of our method on several representative challenging cases. Note that our method successfully separates between the vessels and surrounding structures, including bones, calcifications, and dental implants artifacts.

To cope with the memory requirements of the graph representation, the algorithm divides the scan volume into several block regions with small overlap based on the aorta ROI information. The graph min-cut is then computed for each block independently, and the results are merged together.

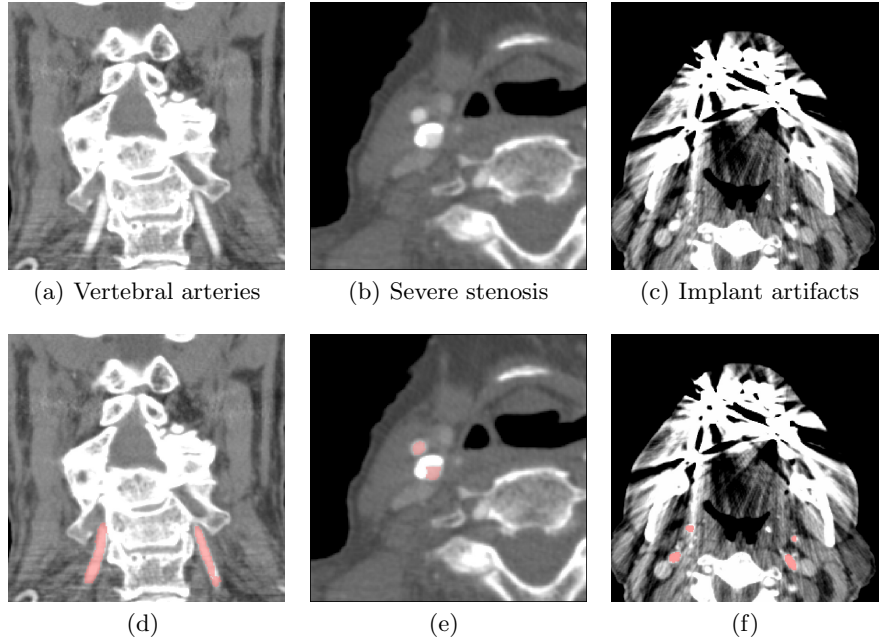


Fig. 3. Segmentation results on several representative challenging datasets: (a)-(c) original CTA images; (d)-(f) 2D view of the segmentation results superimposed on the original CTA slices

2.3 Nearly Automatic Graph-Based Vessel Adding/Removal

Inevitably, the global arteries segmentation step may produce disconnected vessel segments or may miss entire small vessels or include the internal jugular veins (Fig. 4).

To allow the treating physician to fix these flaws interactively, we have developed a spatially constrained graph min-cut interactive editing tool based on the graph min-cut segmentation framework. The nearly automatic tool requires the user to identify two points for each defective or missing vessel. It computes the segmentation of the vessel in two steps: 1) vessel trajectory estimation using a shortest-path algorithm; and, 2) optimal vessel surface computation using spatially constrained graph min-cut.

In the first step, it computes a path inside the vessel as the weighted shortest path between the graph nodes that contain the vessel endpoints. The edge weights compound local image and seed intensity information and vessel path geometric characteristics. In the second step, it constructs a Vessel Region of Interest (VROI) from the vessel path and the estimated vessel radius and computes the min-cut of the subgraph inside it. The min-cut identifies the graph nodes (voxels) at the boundary of the object (vessel) and background, thus producing the desired vessel boundary segmentation. Fig. 5 illustrates the method. We describe each step in detail next.

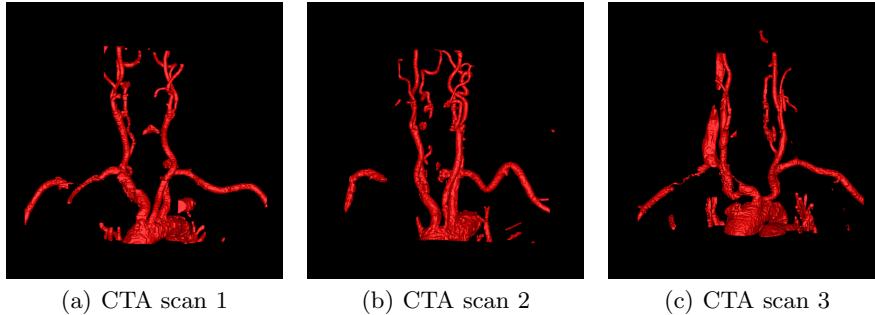


Fig. 4. Spatial visualization of the surface vessel meshes constructed from three CTA scans after automatic segmentation

1. Weighted shortest path computation

The vessel path is computed by finding the weighted shortest path between the vessel seed points v_s and v_f that is inside the vessel. The shortest path is the sequence of edges connecting v_s to v_f for which the sum of its edge weights is minimum. We use Dijkstra’s shortest-path algorithm whose worst-case complexity is $O(n^2)$, where n is the number of image voxels (much less when the vessel seed points are near).

To robustly and accurately find the vessel path, we use a hybrid edge weighting function with intensity and geometric information. The edge weight is the sum of: 1) local intensity difference; 2) seed deviation intensity difference; 3) path smoothness; and 4) path length penalty.

The local intensity difference term is the squared difference of the edge voxel intensity values:

$$(I(v_i) - I(v_j))^2 \quad (6)$$

Since its value is large at boundary crossings, it prevents the path from leaving the vessel region.

The seed deviation intensity difference term is the sum of the relative squared differences of the seeds and edge end voxel intensity values:

$$(I(v_j) - I(v_s))^2 + (I(v_j) - I(v_t))^2 \quad (7)$$

This term prevents the edges in the path from diverging too much from the intensity values of the user-selected seed points. Its effect is to prevent the path to move along locally smooth tissues with low edge weights rather than moving inside the noisy vessel.

The path smoothness term is the angle between the edge voxels gradient directions:

$$|\cos^{-1}(\nabla v_i \cdot \nabla v_j)| \quad (8)$$

where ∇ is the normalized voxel gradient. This term prevents edges with large gradient differences to be added to the path.

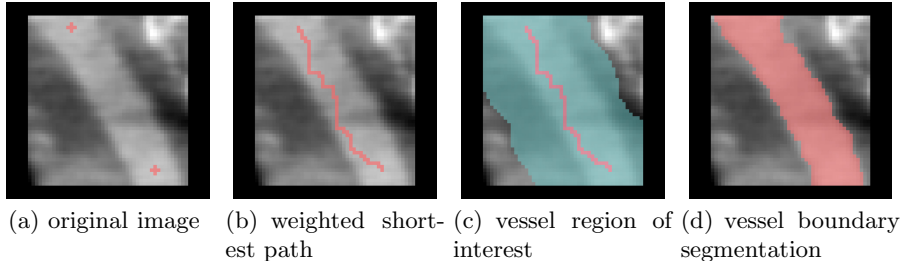


Fig. 5. Illustration of the segmentation process on a clinical coronal CTA slice of the carotid artery: (a) detail of the original image showing the start and end vessel seed points (cross); (b) weighted shortest path between the two seeds; (c) vessel region of interest, and; (d) vessel boundary segmentation

The path length term is the Manhattan distance contribution of the edge. This term penalizes long paths.

2. Optimal vessel boundary segmentation

The vessel boundary segmentation step starts by defining a Vessel Region of Interest (VROI) from the vessel path and the estimated vessel radius. It then updates the graph edge weights according to the VROI and computes the graph min-cut to identify vessel boundary voxels [14].

The VROI is computed as follows. First, two VROI boundaries are computed from each seed point by taking the perpendicular of the path at the seed point and symmetrically extending it by twice the estimated vessel radius. Within the band defined by the two line segments, all nodes that are at a distance of twice the estimated vessel radius from the vessel path are included in the VROI.

Next, the vessel boundary segmentation is formulated as a min-cut problem over the corresponding graph. We use the same graph representation as in the previous step, with two additional terminal nodes v_s, v_t corresponding to object and background classes, respectively. In addition to the edges between voxels (v_i, v_j) , we add two edges for each voxel node v_i : $(v_i, v_s), (v_i, v_t)$. The edges (v_i, v_s) are from voxels to the object terminal node and the edges (v_i, v_t) are from voxels to the background terminal node.

Edges weights are assigned as follows. Edge weights $w(v_i, v_s)$ represent the probability that voxel v_i is related to the vessels (object) or to the background:

$$w(v_i, v_s) = \exp\left(-\frac{I(v_i) - \mu_p}{\sigma_p}\right)^2 \cdot k \quad (9)$$

where μ_p is the intensity mean value along the computed path, σ_p is the standard deviation and k is a scalar multiplier that depends on the distance between the current voxel v_i and the computed path. It represents the probability that the voxel belongs to the object class based on voxel's intensity v_i and object's mean intensity value combined with spatial information that prefer voxels that are closer to the path computed before.

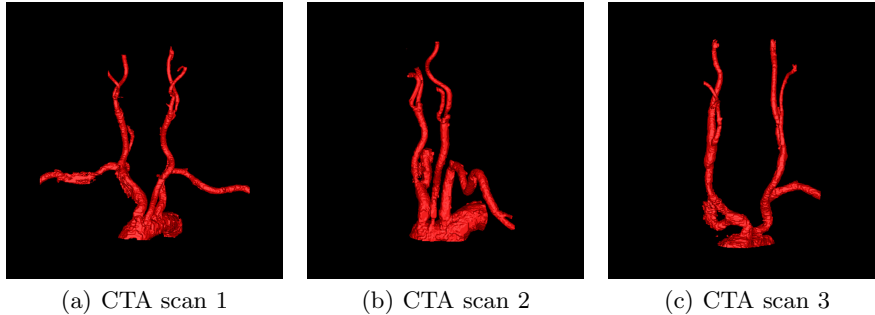


Fig. 6. Spatial visualization of the surface vessel meshes constructed from three CTA scans after the nearly automatic refinement. 3D movies are available at: <http://www.cs.huji.ac.il/~freiman/vessels-cut>

Edge weights $w(v_i, v_t)$ represent the probability of each voxel to belong to background:

$$w(v_i, v_t) = 1 - w(v_i, v_s) \quad (10)$$

We use the inverse of the object weight $w(v_i, v_s)$, instead of explicit modeling of the background intensity.

Edges weight $w(v_i, v_j)$ represent the magnitude of the local gradient between the adjacent voxels:

$$w(v_i, v_j) = \exp\left(-\frac{I(v_i) - I(v_j)}{\sigma_p}\right)^2 \quad (11)$$

The optimal surface that separates the image into a vessel object and background is the min-cut at the resulting graph.

3 Experimental Results

We evaluate our segmentation method on 30 carotid arteries obtained from 15 clinical CTA scans acquired at two sites, each with its CT machine (Siemens and GE). For the first ten scans, patients were administered 100cc of non-iodinated contrast agent with a rapid injection aid at 3-4cc per sec. These CTAs have $512 \times 512 \times 750$ voxels of size $0.5 \times 0.5 \times 0.55mm^3$. For the remaining five scans, patients were administered 125cc of non-iodinated contrast agent with a rapid injection aid at 5cc per sec. These CTAs have $512 \times 512 \times 120$ voxels of size $0.35 \times 0.35 \times 1.25mm^3$.

The scans include varying levels of stenosis and dental implants streaking artifacts. Ground-truth segmentations of the arteries and vessels were obtained manually by a 3D segmentation expert and validated by an expert radiologist.

Each volume was divided into five regions: 1) aortic arch; 2) subclavian arteries; 3) common carotid arteries; 4) common carotid bifurcation into internal

Table 1. Comparison metrics and scores for 15 CTA scans. The first column is the segment type. The second column is the Absolute Volume Difference (AVD) from the ground-truth in %. The third column is the Average Symmetric Surface Distance (ASSD) in mm. The fourth is the Root Mean Square Symmetric Surface Distance (RMS SSD) in mm. The fifth column is the Maximal Symmetric Surface Distance (MSSD) in mm. The sixth column is the Volumetric Overlap Error (VOE) in %.

	AVD (%)		ASSD (mm)		RMS (mm)		MSSD (mm)		VOE	
	mean	std	mean	std	mean	std	mean	std	mean	std
Aortic Arch	14.95	9.55	1.03	0.56	1.58	0.79	16.48	24.54	19.06	8.67
Subclavian arteries	23.99	13.66	0.74	0.45	1.30	1.03	9.06	5.28	33.09	10.28
Common carotid	12.74	8.64	0.29	0.14	0.55	0.20	5.63	4.10	18.07	6.92
Carotid bifurcation	16.69	13.25	0.43	0.39	0.71	0.74	4.37	4.24	26.59	18.75
Internal & external carotids	24.65	19.40	0.70	0.58	1.47	1.29	12.04	8.82	40.74	24.65
Entire arteries	16.43	9.87	0.79	0.25	1.68	0.94	20.51	7.81	24.11	6.95

and external carotid arteries; and, 5) internal and external carotid arteries. The bifurcation region was defined as 25mm above and below the bifurcation. Segmentation results of each region were evaluated separately following the methodology in [17]. Both volumetric, and surface based measures were computed. Fig 6 shows three examples of the vessels segmentation using our method. Note the high quality of the proposed method segmentation results.

Table 1 summarizes the results of the 15 cases for individual segments and for all segments. Our method successfully segmented all datasets accurately without any failure from datasets with both mild and severe stenosis and with calcifications, without any parameter tuning, unlike the results reported on [8] for CTA images. The accuracy of our method around the carotid bifurcation is almost twice better than the results reported in [8]. Our overall accuracy is similar to the results reported in [8], while segmenting much more challenging regions, including the subclavian, aortic-arch, and internal and external carotid secondary bifurcations. The segmentation performance difference around the carotid bifurcation and of other parts of the carotid system stems from the varying noise and imaging artifacts caused by the intensity degradation near the shoulders bones and dental implants on the upper level of the internal and external carotid arteries.

The automatic segmentation mean computation time on a standard PC dual-core 2.4GHz with 3GB of memory machine was 470secs (std=212 secs) for the ten high resolution scans, and 154 secs (std=12 secs) for the five lower resolution scans. The nearly automatic refinement stage required on average 10 seeds and

took the radiologist less than 2mins for each case with no technical support. This sets apart our method from existing semi-automatic and interactive methods which are more laborious and time consuming. These results indicate that our method is accurate, robust and easy to use for patient specific modeling of the carotid arteries system.

4 Conclusion

We have developed a nearly automatic graph-based method for patient-specific modeling of the aorta and the carotid, vertebral, and subclavian arteries for patient-specific simulations from CTA scans. The method automatically generates a vessel segmentation which is then refined by the treating physician with an easy-to-use tool to produce a mesh for simulation. Our results show that the proposed method is accurate, robust, easy to use, and can be integrated into existing simulators for patient-specific simulations. We are currently integrating the algorithm into the simulation platform and are extending it to other vascular structures and procedures, such as liver vessels and abdominal aortic aneurism.

Acknowledgment

This research is supported in part by MAGNETON grant 38652 from the Israeli Ministry of Trade and Industry.

References

1. Kirbas, C., Quek, F.: A review of vessel extraction techniques and algorithms. *ACM Comput. Surv.* 36(2), 81–121 (2004)
2. Kim, D., Park, J.: Connectivity-based local adaptive thresholding for carotid artery segmentation using MRA images. *Image and Vis. Comp.* 23(14), 1277–1287 (2005)
3. Frangi, A., Niessen, W., Vincken, K., Viergever, M.: Multiscale vessel enhancement filtering. In: Wells, W.M., Colchester, A.C.F., Delp, S.L. (eds.) *MICCAI 1998*. LNCS, vol. 1496, pp. 130–137. Springer, Heidelberg (1998)
4. Lorigo, L., et al.: Curves: Curve evolution for vessel segmentation. *Med. Image Anal.* 5, 195–206 (2001)
5. Nain, D., Yezzi, A., Turk, G.: Vessel segmentation using a shape driven flow. In: Barillot, C., Haynor, D.R., Hellier, P. (eds.) *MICCAI 2004*. LNCS, vol. 3216, pp. 51–59. Springer, Heidelberg (2004)
6. Lekadir, K., Merrifield, R., Guang-Zhong, Y.: Outlier detection and handling for robust 3-D active shape models search. *IEEE Trans. Med. Imaging* 26(2), 212–222 (2007)
7. Schaap, M., et al.: Bayesian tracking of tubular structures and its application to carotid arteries in CTA. In: Ayache, N., Ourselin, S., Maeder, A. (eds.) *MICCAI 2007, Part II*. LNCS, vol. 4792, pp. 562–570. Springer, Heidelberg (2007)
8. Manniesing, R., Viergever, M., Niessen, W.: Vessel axis tracking using topology constrained surface evolution. *IEEE Trans. Med. Imaging* 26(3), 309–316 (2007)

9. Friman, O., Hindennach, M., Peitgen, H.O.: Template-based multiple hypotheses tracking of small vessels. In: Proc. of the 5th IEEE Int. Symp. on Biomedical Imaging: From Nano to Macro. ISBI 2008, pp. 1047–1050 (2008)
10. Boykov, Y., Funka-Lea, G.: Graph cuts and efficient n-d image segmentation. *Int. J. of Comp. Vision* 70(2), 109–131 (2006)
11. Kang, L., Xiaodong, W., Chen, D., Sonka, M.: Optimal surface segmentation in volumetric images - a graph-theoretic approach. *IEEE Trans. Patt. Anal. and Mach. Intell.* 28(1), 119–134 (2006)
12. Slabaugh, G., Unal, G.: Graph cuts segmentation using an elliptical shape prior. In: Proc. of the 2005 IEEE Int. Conf. on Image Processing, ICIP 2005, vol. 2, pp. 1222–1225 (2005)
13. Sinop, A., Grady, L.: Accurate banded graph cut segmentation of thin structures using laplacian pyramids. In: Larsen, R., Nielsen, M., Sporring, J. (eds.) MICCAI 2006. LNCS, vol. 4191, pp. 896–903. Springer, Heidelberg (2006)
14. Ning, X., Narendra, A., Ravi, B.: Object segmentation using graph cuts based active contours. *Comp. Vision and Image Understanding* 107(3), 210–224 (2007)
15. Rother, C., Kolmogorov, V., Blake, A.: Grabcut: interactive foreground extraction using iterated graph cuts. *ACM Trans. Graph.* 23(3), 309–314 (2004)
16. Freiman, M., Eliassaf, O., Taieb, Y., Joskowicz, L., Sosna, J.: A bayesian approach for liver analysis: Algorithm and validation study. In: Metaxas, D., Axel, L., Fichtinger, G., Székely, G. (eds.) MICCAI 2008, Part I. LNCS, vol. 5241, pp. 85–92. Springer, Heidelberg (2008)
17. Ginneken, B., Heimann, T., Styner, M.: 3D segmentation in the clinic: A grand challenge (2007), <http://www.sliver07.org>